AENEAS Office
44 rue Cambronne
75015 Paris, France
www.penta-eureka.eu
penta@aeneas-office.org
Tel. +33.1 40 64 45 80

EURIPIDES² Office
44 rue Cambronne
75015 Paris, France
www.euripides-eureka.eu
euripides@euripides-eureka.eu
Tel. +33 1 40 64 45 80

WP4: Test & Measurements

Deliverable D4.1: Test & validation methods

Authors: Rob Maaskant

Project Acronym: Innostar
Project Full Title: Innovative Systems and Automated Design for 5G/6G Connectivity and Radar Applications
Project Coordinator: Dr. Jonatan Aronsson
Project Duration: 36 months (Jan. 2022 – Dec. 2024)
Submission Date: 31-May-2023
Dissemination Level: Public

Executive Summary

This report summarizes the work carried out in WP4 over the period Jun 2022 – May 2023 leading up to the first deliverable: D4.1, entitled “Test & validation methods”. Sec. 1 summarizes the proposed objectives of WP4, the expected results and lists of tasks. The tasks contributing to this deliverable are 4.1.1 – 4.2.2. An approximate time planning is included to show how WP4 tasks are being carried out over time to reach to the three deliverables in WP4.

More specifically, Sec. 2 summarizes the results that led to the first deliverable. The TU/e and NXP have collaborated and determined the sources of uncertainty for typical antennas at 100+ GHz systems. Reflection from the antenna flange is one of them. Solutions to overcome structural reflections have been proposed and additional solutions (such as alignment and calibration) are being examined. It was also found that the antenna gain could differ a few dB simply by accurately re-measuring the antenna dimensions without relying on the manufacturer specifications. Hence, manufacturing tolerances turned out to play an important role. A calibration technique to accurately account for losses is under development. Discussion on validation has been ongoing with WP3 and WP5.

At both Chalmers and NXP efforts have been undertaken to develop a technique for measuring antenna-in-package characteristics in a contactless manner, over-the-air. Chalmers uses the WIN process, while NXP their internal SiGe process. Chalmers has developed a method for extracting the S-parameters of antenna-array-in-package modules. During that process, problems have been identified (see Sec 2.2) that have partly been solved but also need further investigation. Besides the theoretical formulation, an on-chip load-switching network was implemented that was also measured and connected to the antenna-on-chip. Practical problems were identified that were possible to mitigate to some extent. The results for a single antenna element are about to be published after which the array case will follow. A next measurement campaign is being planned.

While the TU/e is mainly focussing on measurement uncertainties, Chalmers/NXP develops active antenna in package, Fraunhofer ENAS is developing the corresponding 90 to 140 GHz anechoic measurement system. Fraunhofer’s existing near-field scanner is being scaled up; new front-end hardware has been ordered. Furthermore, the design of a new probe is underway alongside the development of a probe-calibration/compensation procedure. Initial field tests are to be expected in Q3 2023. A test antenna from the consortium can then be used (e.g. from WP2, TU/e, Chalmers).

Besides Fraunhofer’s near-field anechoic test environment, Bluetest has also scaled-up their reverberation chamber product to 100+ GHz frequencies. The design (mechanical and RF aspects) has been completed and the purchase of components has been made. The assembly of components has been carried out and mechanical parts have been checked from their RF performance point-of-view. The mounting of the HF-stirrer has also taken place and the programming of the required electronic parts has been completed. Functional RF tests are ongoing and the first RF validation through measurements are being planned using a test antenna from the consortium (e.g. WP2).

The EMC group at the TU/e has made an extensive overview on the potential sources of interference that can exist, the types of coupling mechanisms (capacitive, inductive, radiative, conductive), propagation through package substrate, reflections/refractions of fields, and various types of radiation

have been discussed. Afterwards, the potential mitigation techniques at mm-wave frequencies have been summarized (shielding, filtering and decoupling, grounding, routing and isolation. Also, the applicability of the LEGO simulation software has been pointed out for modelling these effects. LEGO is currently under development in the Anterra consortium (Netherlands, Canada). The TANGO framework (Multi-Load Electromagnetic Wave Exchange Framework) has been proposed as the way forward to e.g. measure efficiencies and noise propagation effects. For this purpose a reverberation environment is being considered, first at lower frequencies. Note that the complementary mm-wave reverb is under development at Bluetest.

WP4 is generally on-track. There are currently no risks foreseen that could hinder WP4 or the Anterra project from reaching its final goals. Collaborations between partners are already taken place and are now being intensified. The natural next step is to start working towards the software deliverable D4.2 in Q2 of 2024 while finalizing the ongoing work reported in this deliverable D4.1.

Table of contents

Executive Summary 1
Table of contents 2
Abbreviations 3
1. Introduction 4
1.1. Objectives and expected results 4
1.2. Tasks description 5
2. Works Details - Results to be presented in the deliverable 7
2.1.1. Task 4.1.1 Subsystem-level OTA testing methods, including measurement protocols (TU/e, NXPNL) 7
2.2. Task 4.1.2 OTA characterization methods for arrays of co-integrated antenna-IC modules (Chalmers, NXP-NL, Ericsson) 9
2.3. Task 4.1.3 Near-field scanning methods for individual characterization of integrated components (Fraunhofer ENAS) 12
2.4. Task 4.2.1 Test system for the OTA characterization of passive antenna characteristics (Bluetest, Chalmers, Ericsson) 14
2.5. Task 4.2.2 In-package EMC validation methods (TU/e) 16
2.5.1. Propagation path of electromagnetic noise in an MM-wave package 17
2.5.1. Mitigations techniques at mm-waves 19
2.5.2. Prediction and analysis of EM noise in mm-wave packages 21
Simulation and analysis 21
Measurements 21
2.5.3. Development of the TANGO framework (Multi-Load Electromagnetic Wave Exchange Framework) 22
3. Mapping relationships with the other work-packages 25
4. Risks 25
5. Conclusions and Future Work 26
6. References 26
7. Appendices 27
7.1. Mathematical formulation of the Antenna-Array-in-Package measurement method 27
27
28
29
30

Abbreviations

Acronym	Definition	Acronym	Definition

1. Introduction

This report summarizes the work carried out in WP4 over the period Jun 2022 – May 2023 leading up to the deliverable D4.1 entitled “Test & validation methods”. The tasks contributing to this deliverable are 4.1.1 – 4.2.2.

Objectives and expected results

The **main objective of WP4** is to develop the next-generation measurement techniques and platforms for future wireless systems. This includes the development of

- OTA test methods for co-existence and interference with other systems (TU/e)
- OTA validation methods for arrays of IC-based antenna modules (Chalmers)
- Feedback to design flow and EDA tools (CEMWorks, TU/e, IMST, FhG IIS/EAS)

The above-listed methods will be developed based on the system-level specifications and use cases for the wireless communication and autonomous driving demonstrators, including specifications for OTA test parameters. The measurement techniques and platforms will go together with the designs from WP3 and demonstrators from WP5. This will form feedback for iterative improvements in the testing methods.

The **expected results of WP4** are to develop OTA-testing and validation methods for wireless systems at 100+GHz that,

- Enables testing of wireless systems in a time- and cost-efficient manner
- Facilitates definitions of standards and best testing practices for 6G wireless systems
- Enables validation of IC-based antennas, and co-integrated components individually
- Helps maximize co-existence considering both the physical layer and the expected future spectrum re-allocations for several communication channels.
- Enables feedback from measurements to further EDA steps

Two test systems will be designed for the purpose of future commercialization:

- Test system for OTA validation for arrays of IC-based antenna modules (for passive antenna characteristics)
- EMC testing and diagnostics platform

Tasks description

WP4 has the following tasks defined:

4.1 Development of test and validation methods addressing high frequency, wide bandwidth, and integration challenges (TUe, Chalmers, Ericsson, Bluetest, FhG ENAS, NXP-NL). This task will contribute to output O-4: Measurement toolset - Development of test and validation methods	
	4.1.1 Subsystem-level OTA testing methods, including measurement protocols (TU/e, NXPNL) The OTA techniques and platforms will be developed based on the system-level specifications and use cases for the wireless communication demonstrators, including specifications for OTA test parameters. To meet the objectives towards the expected outcomes, we follow these subtasks/steps: (i) Over-the-Air testing methods and best practices for 100+ GHz antenna (sub-)systems for OTA sub-system performance validation; (ii) Techniques for uncertainty estimations for 100+ GHz OTA sub-system measurements enabling well-defined true performance regions, including near-field probing and fixturing effects; (iii) Over-the-Air calibration techniques for antenna sub-systems at 100+ GHz; (iv) Coexistence and interference OTA testing methods at 100+ GHz uncoordinated bands.
	4.1.2 OTA characterization methods for arrays of co-integrated antenna-IC modules (Chalmers, NXP-NL, Ericsson). To meet the objectives towards the expected outcomes, we subdivide these tasks into the following sub-tasks/steps: (i) Formulation of the fast impedance and radiation pattern measurement method for IC-based antenna arrays, based on the illumination of the antenna-IC module by an electromagnetic field which is then backscatters a field that is measured; (ii) Design of the electronically controlled port terminations to include the effect of the backscattered field from the re-radiated field reflecting from the port terminations. This will be done in a contact-less manner to minimize measurement time and eliminate interconnection losses. (iii) Procedure of measuring the backscattered field at different positions in space and post-processing the measurement data for extracting the passive antenna input impedance matrix and embedded element radiation characteristics. (iv) The on-chip impedance tuner will be co-integrated with existing on-chip circuitry or designed as a dedicated IC (WP3 results will be used to identify the most suitable choice).
	4.1.3 Near-field scanning methods for individual characterization of integrated components (Fraunhofer ENAS). Development and construction of a near-field scanner for investigations of the 100GHz+ frequency range. Evaluation of the field data according to magnitude and phase, so that a direct check of the function of individual antenna patch structures is possible. Preparation of the measurement data for further processing in simulation tools.

4.2 Design of Evaluation Boards and Test systems (Chalmers, TU/e, Fraunhofer, IMST, Ericsson). This task will contribute to output O-4: Measurement toolset - Design of evaluation boards and test systems	
	4.2.1 Test system for the OTA characterization of passive antenna characteristics (Chalmers, Ericsson). A test system based on the method developed in Task 4.1.2 will be designed. It will be used for validation of the passive antenna characteristics (e.g. impedance and radiation patterns) of the 100 GHz Antenna Array-in Package (AiP) Demonstrator for Telecom Applications (WP5). This test system will be complementary to the test system developed in Task 4.2.1 for system-level performance characteristics.

	4.2.2 In-package EMC validation methods (TU/e). TU/e will develop techniques, including guidelines and measurement protocols, for in-package EMC validation and testing at mmWave frequencies: appropriate equipment (e.g. field sensors) and consensus measurement techniques (regarding EMC) are missing at such frequencies. In order to EMC-validate the developed demonstrators at mmWave frequencies, we will perform the following research steps: (i) Investigate and develop novel measurement techniques and platforms for EMC testing at mmWave frequencies. (ii) Realize novel EMC diagnosis for in-package propagation of spurious signals and interference.
	4.2.3 Evaluation Board for the multi-physics design flow (IMST). The multi-physics design flow will be demonstrated on a very compact GaN MMIC technology with a BCB front-end for vertical interconnects to front-end electronics. The simulation tool is verified versus high-frequency electrical performance and temperature probed near active component using customized integrated temperature sensors. The probed temperature is compared versus safe operating temperature conditions
	4.2.4 Evaluation boards for RF-IP modules (IMST). Design of evaluation board for characterisation of IMST RF-CMOS analogue front end IPs. Focus on reusability and abstraction of design guidelines. Consideration of parasitic board effects within system testbench. Board performance optimization using EMPIRE. Preparing test software for test automation.

4.3 Comparison of Design Results and Measurement Results (TUe, CEMWorks, IMST, FhG IIS/EAS + ENAS). This task will contribute towards output O-4: Design vs. measurement comparison
4.3.1 Validation and improvement of simulation toolset (CEMWorks, TU/e). In case of poor agreement between simulated design and measurement results: analysis to determine the probable cause(s), in part by additional simulation studies that reveal sensitivities of certain parameters in the model. It may also turn out that some numerical aspect in the model requires extra attention due to the physical dimension of the model and the short wavelength. In case of broad agreement: quantitative analysis of possible discrepancies. In case those discrepancies exceed specified tolerances: refinement of the design and/or test models.
4.3.2 Validation and improvement of mmWave systems cohesive design environment (CEMWorks, FhG IIS/EAS + ENAS Chalmers, IMST). Iteratively improve the cohesive design environment based on the measurement results from WP4 for the designs developed in WP3. The improvements would include improving modelling speed and accuracy for individual building blocks (field simulators, circuit analysis and optimization, black-box modelling), as well as for the interfaces between different simulation domains and toolset integrations.

A timetable of the respective tasks is provided below

Table 1: timetable of WP4 tasks

	2022				2023				2024			
Task	**1-3**	**4-6**	**7-9**	**10-12**	**1-3**	**4-6**	**7-9**	**10-12**	**1-3**	**4-6**	**7-9**	**10-12**
4.1.1						D4.1						
4.1.2						D4.1						
4.1.3						D4.1						
4.2.1						D4.1						
4.2.2						D4.1						
4.2.3										D4.2		
4.2.4										D4.2		
4.3.1												D4.3
4.3.2												D4.3

2. Works Details - Results to be presented in the deliverable

Task 4.1.1 Subsystem-level OTA testing methods, including measurement protocols (TU/e, NXPNL)

The TU/e and NXP have been collaborating to complete the following sub-tasks:

Our first subtask is: “Over-the-Air testing methods and best practices for 100+ GHz antenna (sub-)systems for OTA sub-system performance validation”.

In the frequency range 90 GHz to 140 GHz, we have been determining the far-field gain and radiation pattern of standard gain horn (SGH) antennas and open-ended waveguide (OEWG) antennas, shown in Figure 1, using over-the-Air measurements in the anechoic chamber. In the higher mmWave frequency bands, these two antennas are frequently employed as probe. Additionally, we chose SGH and OEWG antennas because of their simple design and high degree of directionality for performance system validation of our measurement system at 100+ GHz. But as the time goes we will use more complex antennas to validate our system. While performing the measurements, the following observations were made:

- The flange of the antennas has a considerable impact on the radiation pattern and far-field gain of the SGH and OEWG antennas (Figure 2) in the 100+ GHz frequency range. Additionally, it was found that OEWG antenna was more affected by flange reflections than SGH antenna. Therefore, we need to make upgrades either at system or component level to avoid these effects at such high frequencies.

- We tried to reduce the reflections by covering the flange with absorbers, but this only partially resolved the issue. As a result, we are now looking into developing solutions at the component level, which will reduce the reliability on the absorbers.

- We additionally observed reflections arising at the opening edges of the SGH antenna, therefore we are investigating solutions to this issue as well.

Figure 1: The Standard Gain Horn (SGH) antenna and open-ended-waveguide (OEWG) antenna we used for maesurements in the frequency range 90 GHz to 140 GHz.

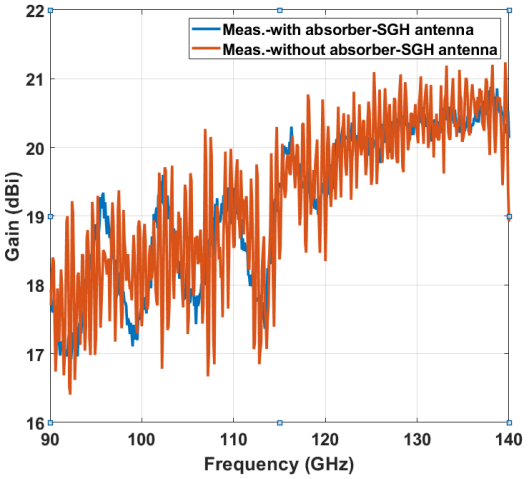

Figure 2: Gain v/s Frequency plot of SGH in the frequency range 90 GHz to 140 GHz showing effect of covering the flange of the antenna with absorbers.

Our second subtask is: “Techniques for uncertainty estimations for 100+ GHz OTA sub-system measurements enabling well-defined true performance regions, including near-field probing and fixturing effects”.

The antenna sub-system is extremely susceptible to perturbations from the environment in the upper mmWave frequency band, notably above 100+ GHz. The uncertainties could arise from both the measurement setup and at the component level. Recently, we have been looking at preliminary set of uncertainties at the component level, and we have carefully examined two of those:

- We found out that the accuracy of the measurement of the far-field gain of the SGH and OEWG antenna, also depends upon how accurate is the method used to estimate the dimensions of the antenna, Figure 3. In our investigation, we evaluated the dimensions of SGH antenna with a caliper and a profile projector (also known as optical comparator), and we found out that it differed by few dB from the gain claimed by the manufacturer.

- Another source of uncertainty is the reflections from the flange of the antenna (explained briefly in sub-task 1), which has a significant impact on gain estimation uncertainty in 100+ GHz range in the far-field region. We are working to improve the alignment and calibration of our measuring equipment to address this problem.

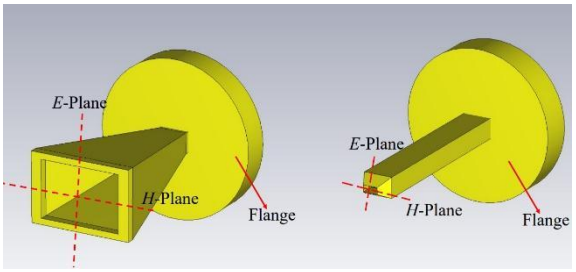

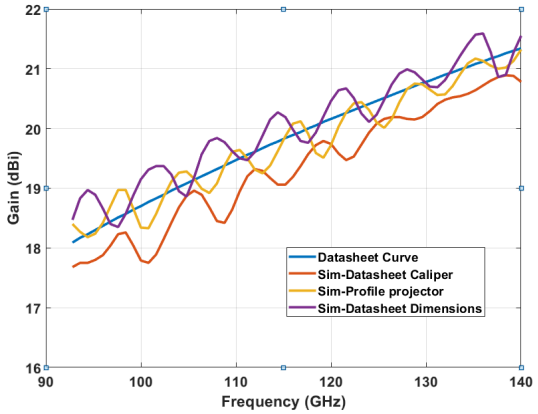

Figure 3: (a) Simulation model of SGH and OEWG antenna (b) Gain v/s Frequency plot of SGH in the frequency range 90 GHz to 140 GHz showing impact of different dimension measurement technique on far-field gain.

Our third sub-task is: “Over-the-Air calibration techniques for antenna sub-systems at 100+ GHz”.

We discovered that full port calibration using Short-Open-Through (SOT) is not possible because we only have a receiver port at the reference antenna end while performing measurements for the SGH and OEWG antenna in the 100+ GHz frequency range in the anechoic chamber measurement setup. Therefore, in order to account for the losses, we took into consideration the free-space path loss and cable loss measurement that we carried out using the setup shown in Figure 4. As a result of this limitation in our measurement setup, we also looked into the uncertainties that might arise.

The above aforementioned issue of calibration technique is subject to further research.

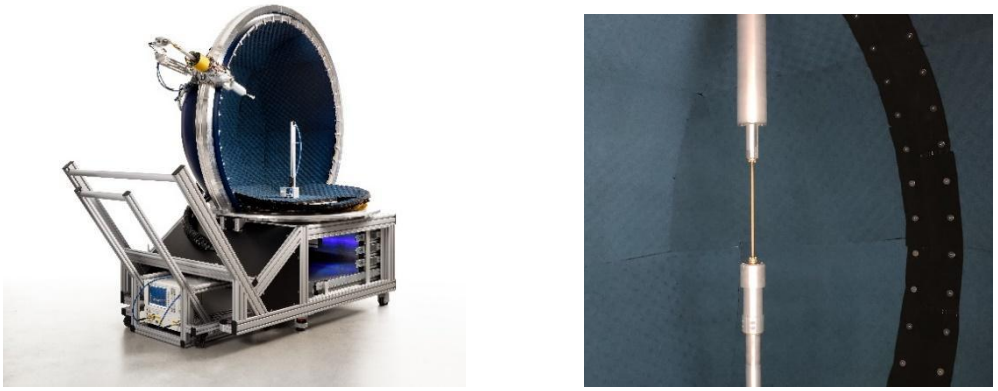

Figure 4: (a) Spherical mmWave anechoic chamber (b) Cable-loss measurement set-up in the anechoic chamber in the frequency range 90 GHz to 140 GHz.

Task 4.1.2 OTA characterization methods for arrays of co-integrated antenna-IC modules (Chalmers, NXP-NL, Ericsson)

Our first objective is: "***Formulation of the fast impedance and radiation pattern measurement method for IC-based antenna arrays, based on the illumination of the antenna-IC module by an electromagnetic field which is then backscatters a field that is measured.***" Appendix 7.1 contains the details of the formulation for both the general array and load matrix case as well as for the two-element DUT and specific load matrix (diagonal matrix). Several observations are being made:

- Four different load terminations per antenna array element are needed to solve the system of nonlinear equations.
- One of these loads is used for re-normalization purposes because this simplifies the solution process
- Yet, there remains a sign-ambiguity in the coupling parameter from chamber antenna to DUT array. This may become a problem since this coupling defines the embedded element pattern of the DUT element in the direction of the chamber antenna. Summing DUT element patterns with wrong signs may yield faulty array patterns. This must be resolved in the future. One way is to resolve for the sign by mapping the measured result onto the simulated result.
- Two solutions are obtained for the coupling between DUT array elements. Once again, this needs to be solved. One solution it to map the measured result onto the simulated result and choose the correct solution.

The above-identified problems are subject to further research.

Our second objective is: "***Design of the electronically controlled port terminations to include the effect of the backscattered field from the re-radiated field reflecting from the port terminations. This will be done in a contact-less manner to minimize measurement time and eliminate interconnection losses.***" Figure 5 shows both the schematic and layout of the designed load-switch in GaAs technology (WIN Semiconductors). It has two in-series pin-diodes open/close sections of the shorted/open grounded coplanar waveguide (GCWG) transmission lines in the MET1, MET2 layers. The two 8-um pin-diode switches result in 4 load states, mostly offset-short loads. A DC current source is connected via the DC pads through wire bonding and the loads are measured on-wafer for different DC bias currents.

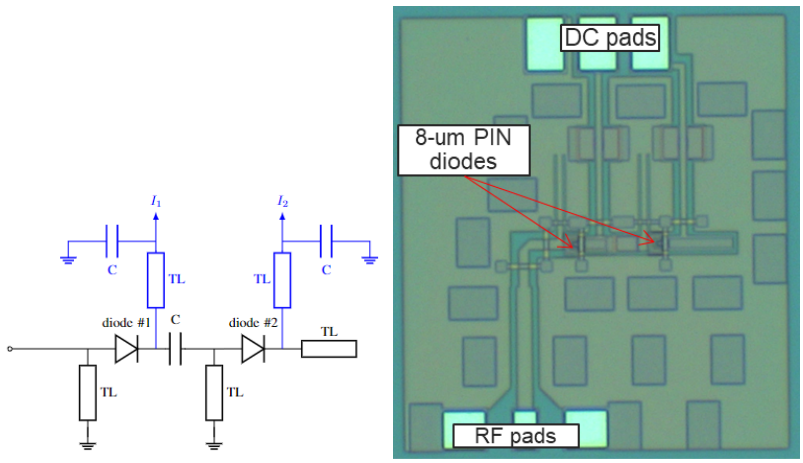

Figure 5: (left) schematic of the load switch; (middle) standalone load switch on wafer; (right) measured load impedances

The solid lines in Figure 5 (right) are the measured results, the dashed ones the simulation and the [i j] – notation denote the diode currents. We found that the switch is less lossy in the measurements and a significant phase shift is observed between the measurements in simulations. We further found that the chosen topology is very sensitive to the PiN diode models. Once diced and assembled, the device overheats instantly at 50 mA current. 10 mA current was used instead, leading to performance degradation since the on-wafer measurement was carried out for 50 mA. Finally, the GSG probe pitch needs to be reduced from 100 um to 75 um, which is more standard with respect to on-the-market GSG probes for D-band applications. It may be that the calibration has suffered from this. A re-design has been planned in the Autumn of 2023.

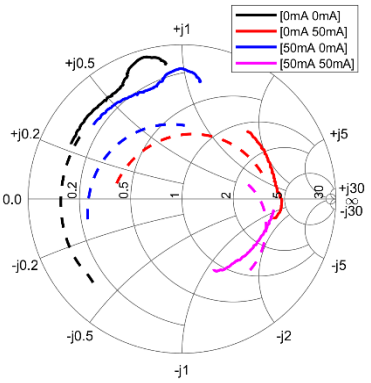

The third objective is: "***Procedure of measuring the backscattered field at different positions in space and post-processing the measurement data for extracting the passive antenna input impedance matrix and embedded element radiation characteristics***." The procedure is described in Appendix 7.1 and has been tested for a single DUT antenna case using the load switch shown above. A single DUT patch antenna was designed as shown in Figure 6 in the same GaAs process. The purpose was to verify the performance of the antenna in an on-wafer measurement. The operation frequency range was chosen from 118.5 – 121.5 GHz (resonance at 120 GHz, 3GHz bandwidth). The antenna is a capacitively-fed cavity-backed patch antenna, where the grounded coplanar waveguide (GCWG) in MET1, MET2 feeding line goes under the patch and terminates in a feeding patch under the radiating patch. A via wall is placed around the patch.

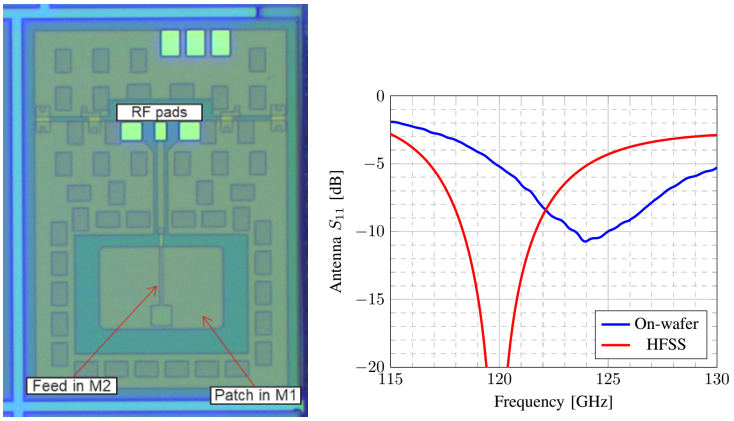

Figure 6: (left) Antenna on chip; (right) on-wafer measured S-parameters and simulations

It can be seen in Figure 6 that the resonance frequency of the fabricated device is shifted from 120 GHz to 125 GHz, which is consistent with the contactless over-the-air measurement (Task 4.2.1). It was checked in simulations that the environment is unlikely to produce such a shift. Furthermore, the antenna is ~2x more resistive in measurement, which is consistent with contactless over-the-air measurement (Task 4.2.1). The feed in M2 was found to be very sensitive to process variation and could lead to this change. A different design was submitted for the next MPW run to test this hypothesis (Autumn 2023).

Our fourth objective is: "***The on-chip impedance tuner will be co-integrated with existing on-chip circuitry or designed as a dedicated IC (WP3 results will be used to identify the most suitable choice).***" For this purpose, we have chosen the operation frequency range 115 – 130 GHz. The goal is to recover the S11 of the DUT antenna in the 115-130 GHz range and to correlate them with on-wafer measurements. Note that the antenna and load switch design in Figure 7 are directly connected at their RF interfaces (RF pads are de-embedded using a TRL procedure).

The measurement setup and results are shown in Figure 7 (middle) and (right), respectively. Details on the single-DUT antenna measurement method can be found in [1], albeit for an off-chip case at much lower frequencies. We have measured S11 of a known reference antenna for different DUT load terminations (controlled by DC). By knowing the response of the load switch, the S11 of the antenna under test can be reconstructed. We observe good correlation between OTA and on-wafer measurements. The measured resonance frequency is within 1GHz (less than 1% deviation). A journal publication is in preparation (letter). Furthermore, a new measurement campaign with improved measurement procedures and adjusted antenna design is planned in the Autumn of 2023.

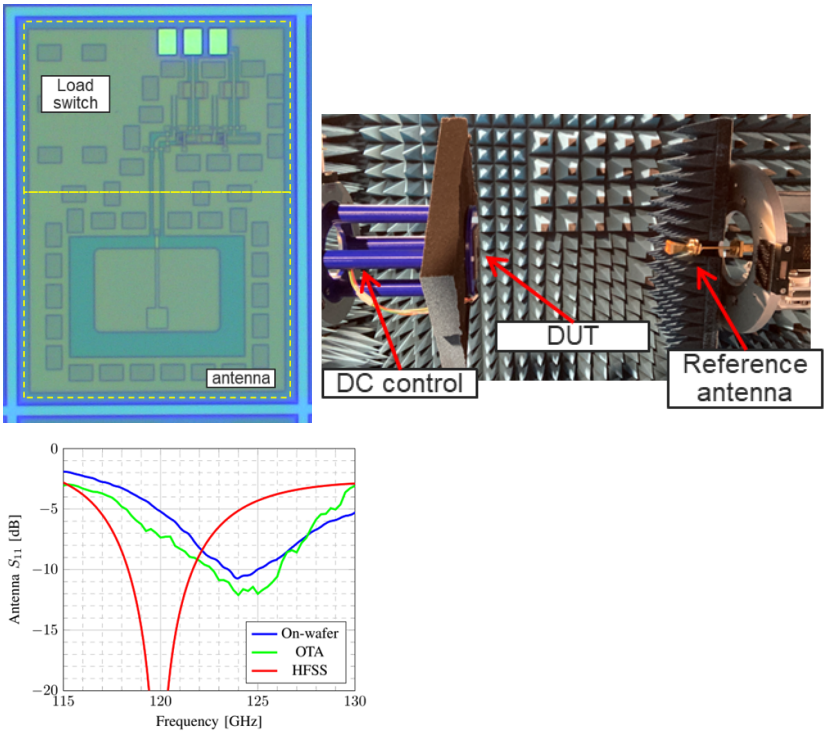

Figure 7: (left) layout of the patch antenna on chip with integrated load switch; (middle) over-the-air measurement setup; (right) measured and simulated S11.

To conclude Task 4.1.2: a theory has been developed for extracting the S-parameters of DUT arrays (see Appendix 7.1). The practical results have been obtained for the single DUT case which enabled us to identify several practicalities, which is an important intermediate step before moving forward with the measurement of a DUT array. The problems that have been identified are:

- Self-heating problems pin-diode switches. Remedy: turn-on/off times need to be controlled.
- Calibration problem of reflective load switch due to larger probe pitch of 100 um. Remedy: order new probes with pitch of 75 um (large lead time of ~20 weeks).
- Sensitive feeding of the patch antenna likely causing a frequency shift. Remedy: new design has been realized and needs to be measured.
- Sign ambiguity exists with the recovery of S-parameters of the DUT arrays. Remedy: no solution has been found yet. A poor man's choice is to resolve the sign by mapping the measurements onto the simulations.

Task 4.1.3 Near-field scanning methods for individual characterization of integrated components (Fraunhofer ENAS)

In task 4.1.3 a near-field scanning (NFS) method is being developed to measure and characterize antennas, passives and other components up to whole electrical systems in the frequency range from 90 to 140 GHz. Near-field scanning can be used to visualize the electromagnetic behaviour of the device-under-test (DUT) and hence to characterize and analyse on a different basis. The electric and magnetic field is determined in certain (usually grid-based) room points to get the spatial distribution of the field-strength. Among others, EMC and radiation/noise sources can be identified, coupling paths can be visualised, antenna characteristics can be derived and verifications of simulations can be

made. Moreover, determined in a specific way, NFS results can be used as simulation source to conduct further investigations of the DUT radiation.
Near-field in this scope of NFS usually means reactive or closer radiative near-field region. A common definition of the reactive to radiative near-field border is

$$f_{nf} \geq 2 \cdot \lambda .$$

For highly radiative and large antennas it is getting larger. For the targeted frequency range this means a λ-range from 3,33 (90 GHz) to 2,14 mm (140 GHz) and therefor a typical maximum vertical measurement distance of 4,28 to 6,66 mm. The actually used measurement distance depends on size, geometry and application of the DUT and the targeted result of the measurement.

The developments of this task are built upon the existing near-field scanner NFS3000 of Fraunhofer ENAS. Its basis is 3-axis portal robot with a measurement area of 50x80x50 cm³ along with a maximum step size 1 µm, which is necessary for precise positioning of near-field probes for small DUTs. The current measurement equipment consists of a two-channel Vector Signal Analyser with a maximum frequency of 50 GHz. The two-channel design is needed to get achieve a phase-related measurement to determine amplitude and phase in every measurement point. With the usage of front-ends (frequency extensions) the maximum frequency currently is at 90 GHz. Hence, new front-ends up to 140 GHz were ordered and will be implemented into the existing measurement chain. The expected shipping is within Q3 2023.

For the described purpose, the front-ends have the following (basic) specifications:

- Frequency range of 90 to 140 GHz
- WR8 waveguide connector for RF
- 2,4 mm connector for IF
- Up- and down-conversion to a maximum IF of 50 GHz

The final measurement chain then will consist of a PC to control everything, the two channel VSA, the available SPUs to pre-process data (LNA, switches) and the front-ends with probes.

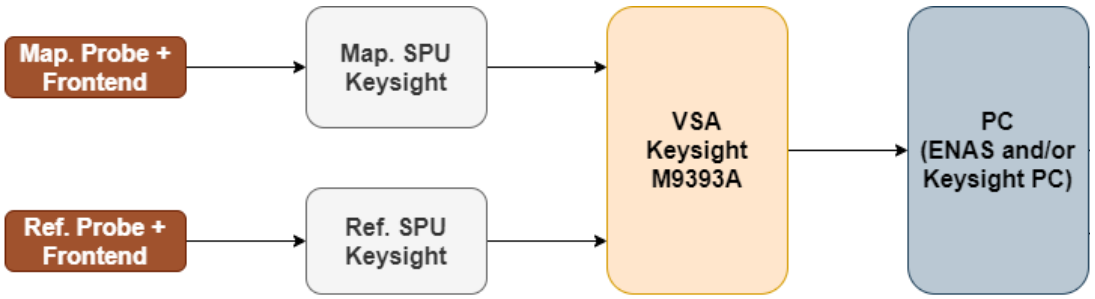

Figure 8 - Measurement chain of the NFS3000 for 90 to 140 GHz

No less important are the near-field probes. Potential near-field probes will be simulated and tested before they are applied to the NFS system. In the targeted frequency range, probes will be based on waveguide structures. There are several waveguide probes available on the market. To rate the properties and characteristics of possible probes, they are built up in CST as simulation model. Together with a potential test-object, so to say “simulated measurements” are performed. In Figure 9 a simulation setup with a probes (left) and a horn-antenna DUT (right) is shown. In a simulated measurement, like in a real near-field scan, the probe will be moved on a grid across the DUT. Then, at every spatial measurement point, e.g. the power at the probe (or S21) will be evaluated over

frequency, so that finally a 2D picture F_{sim} results. These results can be compared with the original field distribution F_{meas} of the DUT without the occurrence of a probe. In an ideal case, the original one and the simulated are the same, so $F_{meas} = F_{sim}$. So, the smaller the deviation between both results is, the more suitable is the probe for the NFS purpose.

Still, near-field probes always have unideal or parasitic properties, there is usually a difference between both. Using the results from the simulations and later from the real measurements, the probe characteristic can be deconvoluted with a probe function. This means, that the expected result from the simulations and the measurement results are compared to determine the difference between both. The mathematics are based on the Fourier and inverse Fourier transformation, where p/P is the probe function:

$$f_{meas}(x,y) = conv(f_{sim}, p)$$
$$F_{meas}(k_x, k_y) = F_{sim} \cdot P$$
$$\rightarrow P = F_{meas} / F_{sim}$$
$$f_{real}(x,y) = ifft(F_{meas} / P)$$

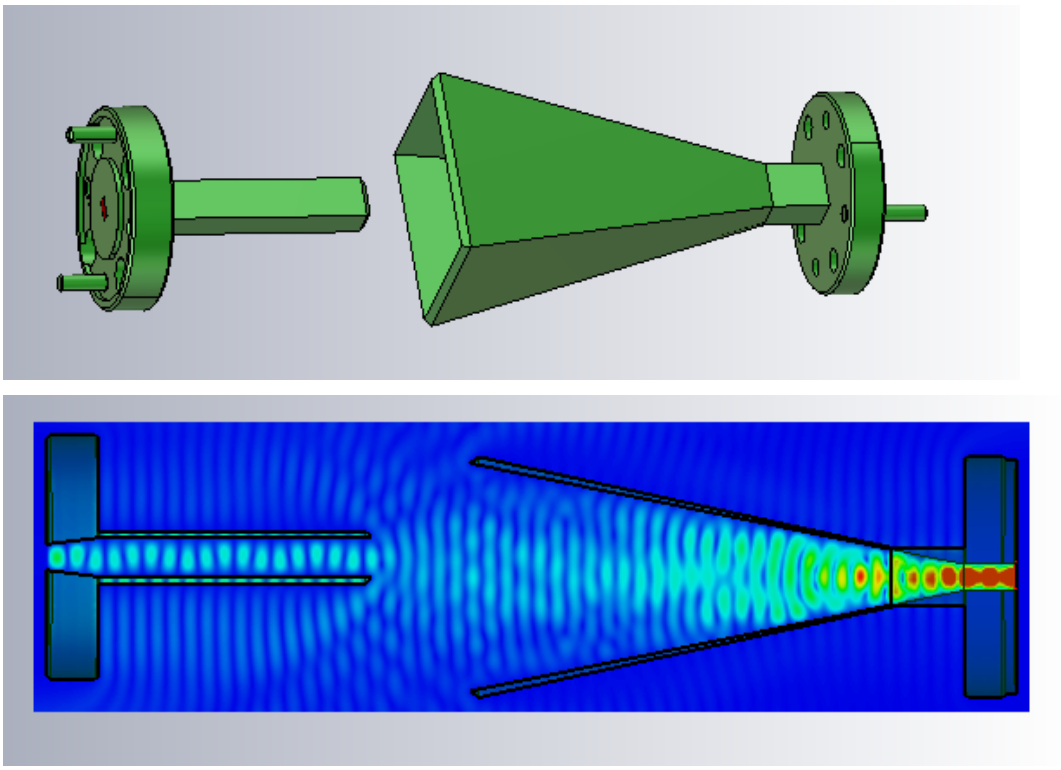

Figure 9 - Test-setup for a simulated measurement

Concluded, the near-field scanning method will be used to characterize and analyse wanted and unwanted radiation of test-devices and finally of the demonstrators of InnoStar. The current state is, that the measurement hardware is ordered and can be tested from the second half of 2023. Meanwhile, simulations on potential probes will be performed to rate their applicability for the NFS purpose. The simulation results will also be used for verification and probe compensation with the real measurement setup.

Task 4.2.1 Test system for the OTA characterization of passive antenna characteristics (Bluetest, Chalmers, Ericsson)

The first objective is: "***A test system based on the method developed in Task 4.1.2 will be designed. It will be used for validation of the passive antenna characteristics (e.g. impedance and radiation patterns) of the 100 GHz Antenna Array-in Package (AiP) Demonstrator for Telecom Applications (WP5).***" For this objective we would like to refer to the results obtained in Section 2.2.

Regarding the second objective: "***A complementary test system will be developed for evaluating system-level performance characteristics.***" A novel mm-wave reverberation test environment is being developed the results of which are shown below.

Aiming for 110 GHz and higher frequencies (HF), Bluetest AB has upgraded its reverberation test systems with a waveguide-based solution so that the characteristics of passive antennas can be measured. The current RTS85HP chamber can perform measurements up to 67 GHz. With this upgrade measurements at frequencies above 110 GHz will be possible. For this upgrade, the steps and actions listed in the following table should be performed. The table also shows the current status for each action item.

Action Items	Status for HF-mode Stirrer
1. Design (mechanical and RF aspects)	• Design of a new structure • Producing several sketches of the mechanical and electronical aspects of the system • Performing RF simulations • Balancing the RF performance and mechanical constraints inherited from the system • Final design confirmed • Status: completed
2. Purchase orders and supplies	• Ordered mechanical, electronic and RF parts needed from action item 1. • Status: completed
3. Assemble and check the mechanical parts and the RF parts from the design point of view	• The new stirrer is assembled, see Figure 10. • From a mechanical point of view, a different slide must be used. The design from a mechanical point of view has been revised and updated. • The newer parts have been ordered and delivered • Status: completed
4. Mounting the HF-stirrer and programming the required electronic parts	• The new stirrer is mounted in the RTS85HP, see Figure 10. • To move the stirrer, the electronic parts are placed and programmed. • Status: competed
5. Software development	• Software development is required to use the HF -mode stirrer as one of the stirrers in the RTS85HP. • Continuous and stepped mode stirring should be available to perform RF tests and validate the solution. • Status:

	▪ Continuous mode stirring: completed ▪ Stepped mode stirring: completed
6. RF tests	• Some test cases are summarized and prepped and additional input might be needed. • Status: under development
7. RF validation through measurements	• This step will be completed after action items 5 and 6. • Status: not completed

Figure 10. New mode stirrer intended for frequencies above 110 GHz. Mounted in RTS85HP chamber at Bluetest AB.

Task 4.2.2 In-package EMC validation methods (TU/e)

EM noise refers to unwanted electrical signals or disturbances that can interfere with the desired operation of electronic devices and systems. The wavelength of the mm-wave (millimetre-waves) ranges from 10 mm (30 GHz) to 1 mm (at 300 GHz). EM noise at mm-waves is specific in several ways compared to EM noise at lower frequencies.

Higher frequency: mm-waves have a frequency range between 30 GHz to 300 GHz, which is much higher than the frequency range of traditional electronics. This high frequency range means that mm-waves are more sensitive to noise and can potentially cause an interference, and the noise is more likely to propagate through structures that may have previously been transparent at lower frequencies. The wavelength of the electromagnetic waves is much shorter, which means that smaller objects and structures can interact with them. This can lead to new coupling mechanisms and propagation paths for EM noise that may not be present at lower frequencies. For example, even small gaps between conductors can act as slot antennas and radiate EM noise.

Small features: mm-wave packages often feature very small components and interconnects, with dimensions on the order of micrometres or even nanometres. This means that even small amounts of EM noise can have a significant impact on the performance of the circuit, and the coupling mechanisms and propagation paths for EM noise are highly dependent on the layout and geometry of the circuit.

Complex circuitry: mm-wave packages often feature complex circuitry, such as mixers, amplifiers, and oscillators, which can have nonlinear behaviour and generate spurious signals that can interfere with other components in the circuit. In addition, the operation of mm-wave circuits is highly

dependent on the precise timing and synchronization of signals, making them more susceptible to noise and interference. Coupling mechanisms and propagation paths for EM noise at mm-waves are more challenging to control and mitigate than these occurring at lower frequencies.

To address these challenges, designers of mm-wave circuits must carefully consider the coupling mechanisms and propagation paths for EMI and employ specialized techniques and tools for EMI analysis and mitigation. These may include specialized simulation software, advanced packaging, and substrate materials, shielding and grounding techniques, and careful layout and interconnect design. Below is a description of the main propagation path of EM- noise. This will be followed by a description of some of the mitigation techniques that can be considered. Finally, techniques available to analyse effect of design choices on EM noise and its mitigation will be summarised. Both simulations and measurements are very challenging. A new hybrid framework to address these challenges will be presented.

Propagation path of electromagnetic noise in an MM-wave package

External sources of EM noise

The propagation of electromagnetic noise in a mm-wave package can originate from external sources, such as *radiated emissions* from nearby electronic devices or power lines, *conducted emissions* from the power supply or ground connections, or *electrostatic discharge* (ESD) events.

Radiated emissions are generated from nearby electronic devices. These emit electromagnetic waves which can couple with nearby mm-wave packages. These emissions can be generated by sources such as power supplies, motors, displays, high-speed digital circuits or other electronic equipment. *Conducted emissions* from power supplies or ground connections: EM noise can also be conducted through the power or ground connections of mm-wave packages. These connections can act as antennas, picking up EMI from external sources and propagating it through the package. *Electrostatic discharge (ESD) events* can generate high-frequency transients that can couple with mm-wave packages and cause damage or malfunction. *Crosstalk between adjacent circuits* within the mm-wave package can also generate EM noise. This can occur through capacitive, inductive, or radiative coupling mechanisms.

Coupling mechanisms

Once an external source of EM noise is present, several coupling mechanisms can occur, such as capacitive coupling, inductive coupling, or radiative coupling.

Capacitive coupling occurs when the electric field from the external source induces an electrical charge on nearby conductive structures, such as interconnects or package substrates. The strength of the capacitive coupling depends on the proximity of the conductive structures, the frequency of the EM noise source, and the dielectric properties of the materials between the source and the conductive structures.

Inductive coupling occurs when the magnetic field from the external source induces a current on nearby conductive structures. The strength of the inductive coupling depends on the proximity of the conductive structures, the frequency of the EM noise source, and the magnetic properties of the materials between the source and the conductive structures.

Radiative coupling occurs when the electromagnetic wave from the external source propagates through free space and couples with the mm-wave package. The strength of the radiative coupling depends on the distance between the EM noise source and the mm-wave package, the frequency of the electromagnetic wave, and the orientation and geometry of the mm-wave package relative to the EM noise source.

Crosstalk coupling occurs when electromagnetic energy from one circuit within the mm-wave package couples with adjacent circuits through mutual capacitance, inductance, or radiation. The strength of the crosstalk coupling depends on the distance between the circuits, the frequency of the signals, and the coupling path between the circuits. Crosstalk coupling can result in a range of undesired effects, such as signal distortion, amplitude modulation, or complete disruption of the circuit operation.

Propagation through package substrate

Once the EM noise has coupled into the mm-wave package, it can propagate through the package substrate. The package substrate is typically made of a dielectric material, which has a different permittivity than air or vacuum. This difference in permittivity can cause the EM noise to propagate with a different velocity and wavelength than it would in free space.

The wavelength of the electromagnetic waves is also small enough that they can propagate through the substrate as surface waves or guided waves, depending on the structure and geometry of the substrate. Surface waves propagate along the surface of the substrate, while guided waves propagate through the substrate between conductive layers or structures. *Surface waves* are more likely to couple with the mm-wave circuit and cause interference, as they propagate along the surface of the substrate and are more susceptible to coupling with nearby conductive structures. Surface waves can be excited by external EM noise sources, such as radiated emissions or conducted noise from nearby electronic equipment and can couple with the mm-wave circuit through capacitive or inductive coupling mechanisms. *Guided waves* are less likely to couple with the mm-wave circuit, as they propagate through the substrate between conductive layers and are more confined to the substrate. Guided waves can be excited by EM noise sources within the mm-wave package, such as switching power supplies or high-speed digital circuits, and can couple with adjacent circuits through capacitive or inductive coupling mechanisms.

Reflections and refractions
Reflections and refraction of EM noise in mm-wave packages refer to the behaviour of EM waves when they encounter boundaries or interfaces within the package. These phenomena can (also) have significant implications for signal integrity. *A reflection* occurs when an EM wave encounters a boundary between two different media, such as the interface between two materials or the transition from air to a substrate, a portion of the wave energy can be reflected into the original medium. The reflection occurs due to the mismatch in impedance between the two media. At mm-wave frequencies, reflections can lead to signal degradation, impedance mismatch, standing waves, and interference. Proper management of reflections is crucial to minimize signal loss, maintain impedance matching, and prevent EMI issues. *A refraction* occurs when an EM wave passes through an interface and changes direction due to the change in propagation speed. This change in direction is governed by Snell's law, which relates the incident angle, refracted angle, and refractive indices of the two media. Refraction can result in the bending of EM waves as they propagate through different materials. In mm-wave packages, refraction can impact signal paths, alter beam propagation angles, and influence the behaviour of waveguides or transmission lines. Understanding and controlling refraction is important for maintaining signal integrity and ensuring proper functionality of mm-wave circuits. Both reflections and refraction can be influenced by various factors, including the dielectric properties of the materials involved, the geometry of the package, and the incidence angle of the EM wave. Designers must consider these factors to minimize signal degradation, optimize power delivery, and mitigate EMI issues.

Another consequence of the wavelength of the electromagnetic waves being comparable to the thickness of the substrate are *dielectric resonance*. This means that the substrate can exhibit resonant behaviour that can couple with other structures on the surface. For example, the dielectric constant of the substrate can create resonances that couple with the metal traces on the surface, leading to new paths for EM noise propagation.

Radiation from mm-wave circuits
The radiation of EM noise in mm-wave packages refers to the emission of EM waves from the package structure or components, which can cause interference with other nearby circuits or external devices.
Any conducting structure or component in the package can act as an *unintentional antenna* and radiate EM waves. This can include traces, vias, connectors, IC leads, or any other metallic structure that has dimensions comparable to the wavelength of the EM waves. These structures can generate radiation due to various factors, such as current flow, voltage gradients, or resonance effects. Unintentional antennas can result in unwanted radiation, causing interference and affecting the performance of nearby circuits.
Aperture radiation occurs when EM waves pass through an opening or aperture in a conductive structure, such as slots, gaps, or openings in shielding enclosures or package walls. The size of the

aperture relative to the wavelength determines the radiation characteristics. Aperture radiation can lead to the leakage of EM waves from the package. For instance, even small gaps between conductors can act as slot antennas and radiate EMI. This can be especially problematic in cases where the gap is unintentional, such as a small separation between two traces on a PCB.
Common-mode radiation arises when there are imbalances or asymmetries in the current distribution within a circuit or transmission line. This can lead to the generation of common-mode currents that radiate EM waves. Common-mode radiation is particularly relevant in differential signalling, where imbalances in the signal paths can result in common-mode currents and subsequent radiation. Proper design techniques, such as balanced transmission line structures and symmetrical circuit layouts, can help minimize common-mode radiation.
The substrate material of the mm-wave package can also contribute to EM radiation. Due to the presence of discontinuities, impedance mismatches, or resonances in the substrate, EM waves can be emitted from the substrate material itself. The *substrate radiation* can couple with nearby circuit components, leading to interference and signal degradation.

1.1.1. Mitigations techniques at mm-waves

Many mitigation techniques exist within mm-wave packages. These are an integral part of the design a such a package and need to be carefully consider during its design. Techniques are summarized in four categories: “shielding”, “filtering and decoupling”, “grounding, routing and isolation”. Each technique is linked to the identified specific propagation paths detailed in the previous section.

Shielding
Shielding the mm-wave package using conductive enclosures or shielding materials can provide a barrier against external EM noise. The enclosure should be properly grounded to ensure effective shielding. Additionally, attention should be given to sealing any gaps or seams to prevent leakage of EM waves (external sources, radiation coupling, reflections, and refractions). Placing a ground plane or shielding layers between the coupled elements can reduce the capacitive coupling by providing a barrier that blocks the electric field between them (capacitive coupling, crosstalk coupling).
Using absorptive materials within the mm-wave package can help attenuate external EM noise. These materials can be placed strategically at specific locations to absorb and dissipate EM energy, reducing the impact of noise coupling.
Filtering and decoupling
Integrating filtering components such as capacitors or inductors can help suppress or re-route unwanted noise and prevent its propagation into the mm-wave circuitry. These components should be strategically placed at input/output ports or power supply lines to attenuate EM noise (in case of external noise source). Proper decoupling of power supply lines is essential to minimize noise coupling.

mm-Wave noise filter design is based on planar transmission lines: they are typically implemented on a PCB substrate using microstrip or coplanar waveguide structures. The filter can for instance consists of two parallel transmission lines (signal lines) separated by a grounded plane or a series of vias. Multi-layer filters: in high-density mm-wave packages, multi-layer filters can be employed to maximize the inductance while minimizing the occupied area. This design utilizes multiple stacked layers of transmission lines and ground planes to achieve the desired inductance and capacitance value. The specific design parameters, such as the dimensions, spacing, and material properties of the filter, depend on the target frequency range, desired impedance, and noise characteristics of the application. Designers often use simulation tools and electromagnetic modelling techniques to optimize filter design for effective noise suppression at the desired frequencies. Using connectors with built-in so called “EMI filters” can help mitigate the radiation coupling at the interface between the mm-wave package and external components. These filtered connectors can attenuate the EM noise before it enters or exits the package.

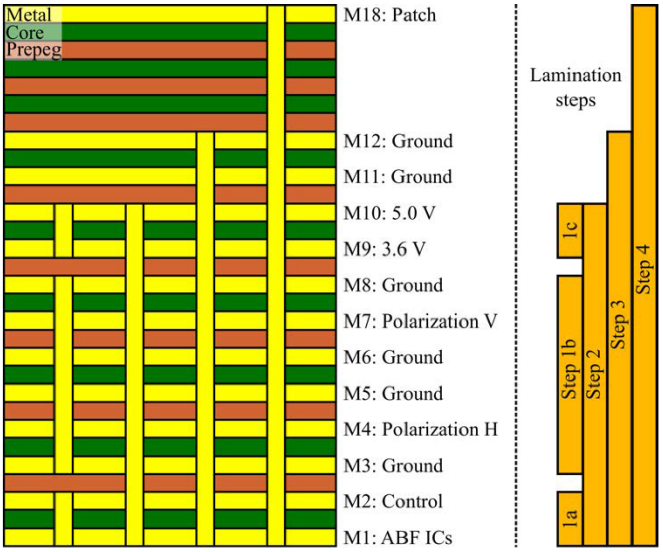

Figure 11: Example of a PCB Stack-up (not to scale) [2]

Grounding, routing, and isolation

Establishing a robust grounding system is crucial for mitigating external EM noise. A low-impedance ground plane should be utilized, and grounding techniques such as star grounding or multi-point grounding can be employed to minimize ground loops and reduce noise coupling. Care should be taken to ensure separate grounds for digital and analogue components to prevent cross-contamination of noise (external source).

Designing the mm-wave package with proper routing techniques can minimize the impact of external EM noise. For example, differential signalling and balanced transmission lines can improve noise immunity. Additionally, proper isolation of sensitive circuitry from noise sources, such as separating digital and analogue sections or using shielding for critical components, can help mitigate external EM noise (external source).

Careful attention should be given to the placement of sensitive components, routing of transmission lines, and minimizing the use of abrupt changes or bends in the signal path. Adequate routing is also an integral part of the reduction strategy of coupling effects, for instance:

- Careful PCB layout techniques, such as maintaining proper spacing between traces and utilizing controlled impedance routing, can reduce crosstalk coupling. More specifically by increasing the spacing between traces or conductive elements, the capacitance between them can be reduced, minimizing the capacitive coupling. This technique is especially useful for minimizing noise coupling in high-density PCB designs. Physically separating and isolating the coupled traces or components can help reduce the inductive coupling.
- Implementing differential signalling with properly matched transmission lines can minimize the impact of inductive coupling. The equal and opposite current flows in the differential pair help cancel out the induced noise.
- Maintaining controlled impedance throughout the PCB layout and transmission lines can minimize reflections and impedance mismatches, which can lead to noise coupling through the substrate. Proper termination techniques, such as series resistors or termination networks, can help control signal integrity and reduce the propagation of noise.
- Low-loss substrate selection: Choosing a low-loss substrate material with a high dielectric constant can help minimize the coupling of noise through the substrate. Low-loss substrates reduce the chances of resonances and attenuate the propagation of noise.
- Substrate decoupling: Placing decoupling capacitors near noise sources or sensitive components on the substrate can help suppress noise coupling. These capacitors provide a low impedance path for high-frequency noise currents to dissipate, reducing their impact on other circuit sections.

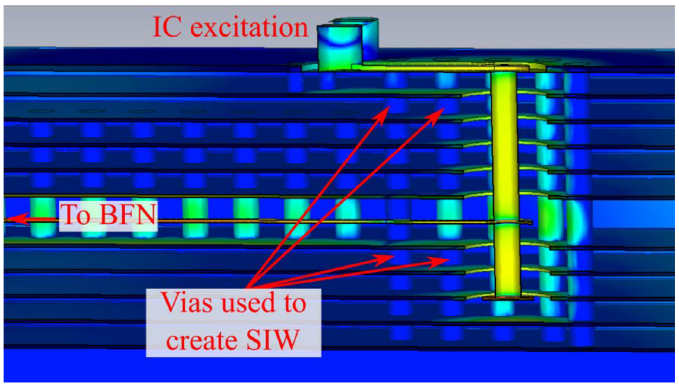

Figure 12: Example on the use of vias to prevent RF leakage [2]

1.1.2. Prediction and analysis of EM noise in mm-wave packages.

Simulation and analysis
Several electromagnetic simulation tools exist such as finite element method (FEM) or finite-difference time-domain (FDTD) simulations or tools with linear embedding via Green's operators (LEGO). They can be used to analyse the propagation of external EM noise within the mm-wave package can help identify potential noise coupling paths and optimize the package design. Through simulations, designers can:

- identify critical coupling paths, optimize design parameters, and assess the effectiveness of mitigation techniques.
- aid in evaluating the effectiveness of different mitigation techniques and optimizing their placement
- can aid in predicting and analysing the radiation behaviour of mm-wave packages. These tools enable designers to identify potential sources of radiation and optimize the design accordingly.

Measurements
Measurements is a key challenge for the analysis of EMC at mm-wave. Parameters such as field strengths, power densities, output power, frequency tolerance, and other regulatory matters are difficult to measure with a known accuracy. The tricky measurement part is that the wavelengths are short, so the beamwidths are very narrow, and getting an accurate measurement of the emitted energy takes a lot more time than standard measurements at lower frequency. These very short wavelengths create a lot of challenges for design and test because of the mechanical precision required for making accurate measurements.

Measurement sensitivity is a specific challenge: mm-wave signals are often very weak due to higher propagation losses and atmospheric absorption. The measurement equipment should have high sensitivity to detect and measure these weak signals accurately. Low noise figures and high dynamic range of the measurement instruments are essential for reliable measurements. *Suitable antennas* for transmitting and receiving MM-wave signals are also necessary. *Accurate calibration* of the measurement equipment is critical for reliable EMC measurements using appropriate calibration standards, reference planes, and calibration kits specific to mm-wave frequencies ensures accurate measurements and compensates for systematic errors in the measurement setup.

The *test environment* should be properly controlled and shielded to prevent interference from external sources and provide an accurate representation of the EMC conditions. Shielded anechoic chambers or specialized RF shielded rooms are often used to minimize external interference and isolate the measurement setup.

Measurement probes at mm-wave frequencies are particularly challenging: the size and design of the probes become critical because of the wavelength. Probes need to be physically small to accurately capture the high-frequency fields, and their design must be optimized for the specific frequency range of interest. mm-Wave signals have a wide bandwidth, often spanning several gigahertz. Probes used

for mm-wave measurements must have sufficient bandwidth to capture the entire frequency range of interest. However, achieving wide bandwidth performance in probes can be challenging due to parasitic effects, resonance, and other impedance-related factors. Signals experience high levels of attenuation as they propagate through the air or other materials. Probes used for mm-wave measurements must have a low insertion loss to minimize signal attenuation and ensure accurate measurements. Minimizing signal loss becomes more challenging as the frequency increases. The calibration becomes also more complex. Accurate calibration requires precise knowledge of the probe's electrical characteristics, including its impedance, radiation pattern, and sensitivity. It requires an integration with measurement equipment: connecting mm-wave probes to measurement equipment, such as vector network analysers or spectrum analysers, can be challenging. The connectors and cables used for these high-frequency measurements must have appropriate impedance matching and low-loss characteristics to maintain signal integrity. Near-field effects also pay an important role with the measurement environment transitions from the far-field to the near-field region. Probes used in the near-field region experience non-uniform field distribution, which can affect their accuracy. Careful consideration and modelling of near-field effects are required to ensure accurate measurements.

1.1.3. Development of the TANGO framework (Multi-Load Electromagnetic Wave Exchange Framework)

Charactering EM noise at mm-wave requires us to think differently especially because the wavelengths are short, so the beamwidths are very narrow. In InnoStar, we aim at developing a specific framework to specifically address the requirements of EM noise propagation characterisation at mm-wave:

- Accurate measurements of EM energy exchanges between all ports of a mm-wave DUT. This implies a complete characterisation of radiative and conductive exchanges between its port. We specifically aim at adding an extra radiative port to each DUT and this novelty needs to be careful considered.
- An ability to adapt to realistic diverse scenarios of noise propagation occurring in unmatched conditions (hence with an impedance at a DUT port potentially different from the standard 50Ohm provided by the VNA).

The first innovation is to add a radiative port to the traditional *parasitic* conducted ports analysis to enable the concept of radiation efficiency for the EM parasitic noise. The Reverberating Chamber (RC) is the most accurate means to measure radiation efficiency as it allows isotropic device measurements. There is no need for device alignment or three-dimensional scans, as there would be in an anechoic chamber. Measuring the radiating efficiency of an antenna in a RC is a known technique but extending this technique to a larger frequency band (so-called “out-of-band” behavior) is a *second innovation*, especially due to the likelihood of resonance frequencies (in the noise propagation) presenting large extrema of (radiation) efficiencies within narrow frequency bands. Particular attention to the accuracy of such measurement is required.

The measurements of all energy transfers occurring between the conducted ports and a radiative port of a DUT are performed with a VNA providing a standard 50 Ohm termination to all ports. Enabling a prediction of these energy transfers (with an extra radiative port) with a set of variable loads at terminations is *third major innovation*. Limits of this multi-load methods need to be identified and the propagation of uncertainties in the prediction requires particular attention.

A high-level overview of the TANGO framework is provided in Figure 13. Ultimately, the TANGO framework aims at characterizing an (N+1) ports DUT with N conductive ports + 1 radiative port as describe in Figure 14.

As described in the previous section on measurements, the development of an accurate RC at mm-wave, along with its probes comes with many challenges. These are being overcome within InnoStar. An example of such a mm-wave RC chamber is shown in Figure 15.

To get started immediately with the development and the validation of the TANGO framework, a choice has been made to start this work with a RC adapted for lower frequencies. Work on accuracy of

radiation efficiency is going [3] [4] : Figure 16 shows an example of accurate radiation efficiency over a large frequency band for a reconfigurable 5G antenna exhibiting narrow-frequency band behaviors. Parasitic effect of probes has already been investigated (Figure 17 and Figure 18). Results are detailed in [3].

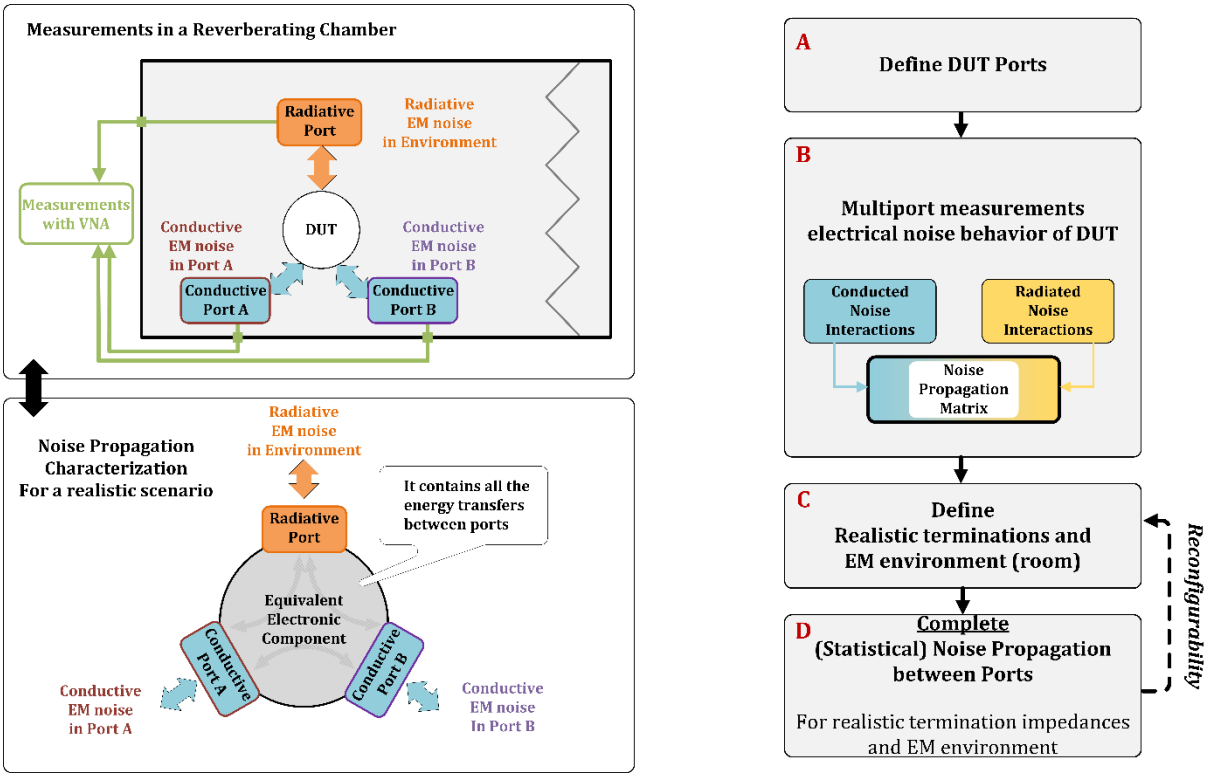

Figure 13: High level overview of the proposed TANGO framework for a realistic characterisation of a mm-wave noise propagation in a DUT

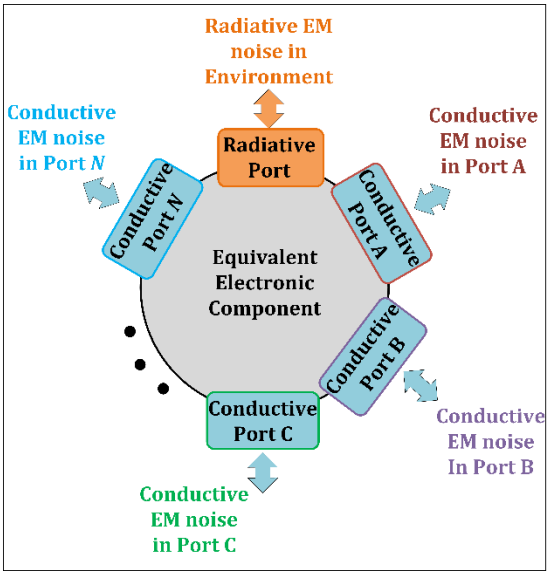

Figure 14: Port allocation in a N ports DUT withing the TANGO framework.

Figure 15: Example of a mm-wave RC chamber in development in TU/e

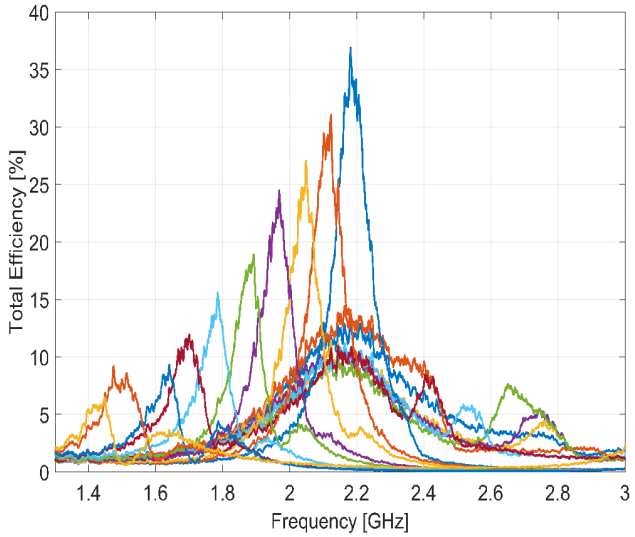

Figure 16: An experimental accurate radiation efficiency for a 5G narrow band reconfigurable antenna measured with my team ***Fehler! Verweisquelle konnte nicht gefunden werden.****], where RC metrics are refined at wavelengths where the chamber is electrically extremely large* ***Es ist eine ungültige Quelle angegeben.***

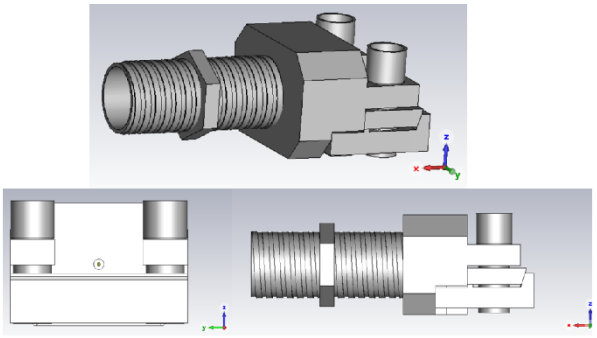

Figure 17: Model of an End-Launch connector in CST [4]

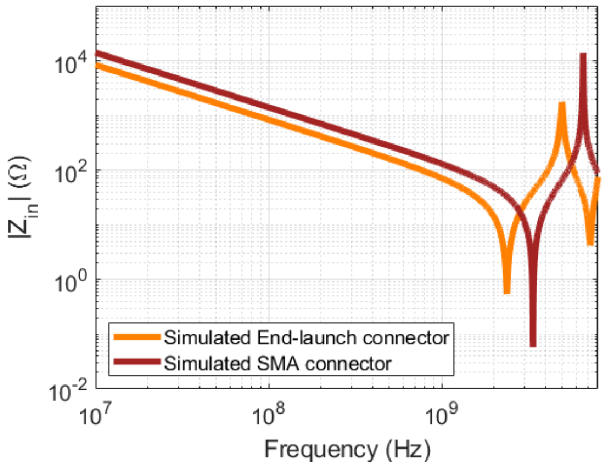

Figure 18: Simulation and comparison of parasitic effects of an End-Launch vs SMA connectors for a lower frequency testbench with the TANGO framework [4]

2. Mapping relationships with the other work-packages

Bluetest:

- For development of OTA tests in the reverberation chamber at frequencies above 110 GHz we require devices that output signals in this frequency range such that we can use them as Device Under Test (DUT). We also need measurement instrumentation that can sample signal at these frequency ranges. To accomplish this, we collaborate with other partners who design and develop such devices. The antennas developed by WP2 are potential candidates. We believe that once Action Item 7 is completed, we should initiate such a collaboration that will benefit both WP4 and WP2. We will contact WP2's partners to accomplish this once the RTS85HP system is ready for such measurements with a new HF-mode stirrer.

TU/e:

- We have been in constant contact with work-package 3 (WP3) and work-package 5 (WP5). We have been following WP3 so that we can learn more about the design and co-optimization of electronic architectures and components, and upgrade our measurement setup to meet their specifications for the precise measurement of the specified subsystem. In a similar vein, we also communicate with WP5, as we will be working on the demonstration of validation and measurement methods on developed hardware. We also give updates and details about the measurement setup in these meetings so that the designs of the antenna sub-systems can align with our capabilities to characterize it

Fraunhofer ENAS:

- To show the feasibility of near-field scanning above 100 GHz, test-devices and demonstrators are needed. Basic DUTs, like a horn antenna or others passives, can be used for testing. The demonstrators and test-structures from the other work-packages should also be included in the measurement campaign with the NFS. Hence, there is contact with other partners from WP2 to WP5. A common measurement campaign could benefit all test-facilities to outline the strength of each measurement method and to compare different results. Finally, NFS results can be compared with field-simulations from other partners for cross-verification and for improvement of designs.

3. Risks

Bluetest:

- Has already overcome one of the challenges and risks that we predicted in the design phase of the HF -mode stirrer project, i.e., action item 3. This has delayed the project by about 8 weeks, but we are back on track.
- Another risk is a potential problem in running the RF test and validation phase, which could be due to design and/or RF parts and instrumentation being limited at such high frequencies. This type of risk is unavoidable, requires further investigation, and may incur additional costs, such as purchasing new RF and mechanical parts, which will also impact delivery time.

TU/e:

- There was a delay in hiring the PhD candidate w.r.t. the starting date of the project innostar. The hired PhD candidate Purnima Yadav started working on this project on 1st September, 2022.
- The 100 GHz Antenna array-in-package (AiP) demonstration hardware has been delayed in WP3, which may affect our anticipated schedule for the measurements of this hardware. To prevent this delay, we are talking to our partners in WP3 about the potential of using a different DUT with a similar architecture so that we can test our measurement set-up.

Fraunhofer ENAS

- The German project started with a delay of 3 months. For now, there is no issue with this delay as some of the simulation work can be shifted to an earlier stage.
- The cost for the new measurement equipment is a bit higher then in the PO phase and therefore usage of funding needs to shift a bit from PM/travel to invest. The amount shifted should not be any problem for the overall target at Fraunhofer ENAS.

As of yet, and generally speaking, there are no risks foreseen that could hinder the Anterra project from reaching its final goals.

4. Conclusions and Future Work

The tasks that have contributed to the present deliverable D4.1 are:

4.1.1 Subsystem-level OTA testing methods, including measurement protocols (TU/e, NXPNL)
4.1.2 OTA characterization methods for arrays of co-integrated antenna-IC modules (Chalmers, NXP-NL, Ericsson)
4.1.3 Near-field scanning methods for individual characterization of integrated components (Fraunhofer ENAS)
4.2.1 Test system for the OTA characterization of passive antenna characteristics (Chalmers, Ericsson).
4.2.2 In-package EMC validation methods (TU/e)

Novel measurement methods have been proposed for future mm-wave antennas characterized in both reverberation and near-field anechoic chamber environments, and also for antenna-on-chip systems. Measurement uncertainties and electromagnetic compatibility issues have been identified. Interference mitigation solutions have been proposed as well as various calibration techniques to overcome these challenges.

WP4 is generally on-track. There are currently no risks foreseen that could hinder WP4 or the Anterra project from reaching its final goals. Collaborations between partners are already taken place and are now being intensified to allow for cross validation and hardware sharing. The natural next step is to start working towards the software deliverable D4.2 in Q2 of 2024 while finalizing the ongoing work reported in this deliverable D4.1.

5. References

[1] A. J. Van Den Biggelaar et al., "Verification of a Contactless Characterization Method for Millimeter-Wave Integrated Antennas," *IEEE Transactions on Antennas and Propagation,* pp. 3358-3365, 2020.

[2] L. A. Bronckers, A. Roc'h and A. B. Smolders, "A New Design Method for Frequency-Reconfigurable Antennas Using Multiple Tuning Components," *IEEE Transactions on Antennas and Propagation,* vol. 67, no. 12, pp. 7285-7295, 2019.

[3] L. A. Bronckers, K. A. Remley, B. F. Jamroz, A. Roc'h and A. B. Smolders, "Uncertainty in Reverberation-Chamber Antenna-Efficiency Measurements in the Presence of a Phantom," *IEEE Transactions on Antennas and Propagation,* vol. 68, no. 6, pp. 4904-4915, 2020.

[4] M. Khorramizadeh et al, "Assessment of a Test setup on the Impedance Measurement of Cables," in *EMC Europe*, 2023.

6. Appendices

Mathematical formulation of the Antenna-Array-in-Package measurement method

1 S-parameter Model

Consider the chamber antenna (CA) that illuminates and subsequently measures the backscattered field of a DUT antenna array in Fig. 1. The DUT can be an Antenna-Array-on-Chip or Antenna-Array-in-Package without physically accissible ports.

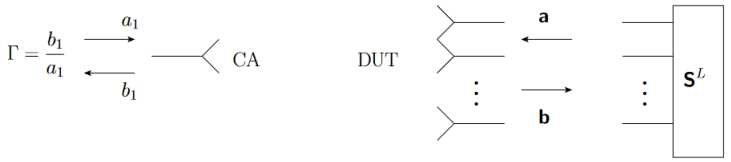

Figure 1: Measurement setup.

We are interested in expressing the measured reflection coefficient Γ in terms of the on-chip load matrix $\mathbf{S}^{\mathrm{L}}$. Using S-parameters:

$$\begin{pmatrix} b_1 \\ \mathbf{b} \end{pmatrix} = \begin{pmatrix} S_{11} & \mathbf{S}^{\mathrm{CA,DUT}} \\ \mathbf{S}^{\mathrm{DUT,CA}} & \mathbf{S}^{\mathrm{DUT,DUT}} \end{pmatrix} \begin{pmatrix} a_1 \\ \mathbf{a} \end{pmatrix} \tag{1}$$

and

$$\mathbf{a} = \mathbf{S}^{\mathrm{L}}\mathbf{b} \tag{2}$$

That is, when rewriting (1) as

$$b_1 = S_{11}a_1 + \mathbf{S}^{\mathrm{CA,DUT}}\mathbf{a} \tag{3a}$$
$$\mathbf{b} = \mathbf{S}^{\mathrm{DUT,CA}}a_1 + \mathbf{S}^{\mathrm{DUT,DUT}}\mathbf{a} \tag{3b}$$

and after multiplying (3b) by $\mathbf{S}^{\mathrm{L}}$ one obtains

$$\mathbf{S}^{\mathrm{L}}\mathbf{b} = \mathbf{S}^{\mathrm{L}}\mathbf{S}^{\mathrm{DUT,CA}}a_1 + \mathbf{S}^{\mathrm{L}}\mathbf{S}^{\mathrm{DUT,DUT}}\mathbf{a} \tag{4}$$

which can be rewritten with the help of (2) as

$$\mathbf{a} = \mathbf{S}^{\mathrm{L}}\mathbf{S}^{\mathrm{DUT,CA}}a_1 + \mathbf{S}^{\mathrm{L}}\mathbf{S}^{\mathrm{DUT,DUT}}\mathbf{a} \tag{5}$$

which can be solved for $\mathbf{a}$, yielding

$$\mathbf{a} = \left(\mathbf{I} - \mathbf{S}^{\mathrm{L}}\mathbf{S}^{\mathrm{DUT,DUT}}\right)^{-1}\mathbf{S}^{\mathrm{L}}\mathbf{S}^{\mathrm{DUT,CA}}a_1 \tag{6}$$

which is then substituted in (3a) to arrive at

$$b_1 = S_{11}a_1 + \mathbf{S}^{\mathrm{CA,DUT}}\left(\mathbf{I} - \mathbf{S}^{\mathrm{L}}\mathbf{S}^{\mathrm{DUT,DUT}}\right)^{-1}\mathbf{S}^{\mathrm{L}}\mathbf{S}^{\mathrm{DUT,CA}}a_1 \tag{7}$$

Finally, since $\Gamma = b_1/a_1$, the measured reflection coefficient at the chamber antenna is, fort a general DUT array and load matrix,

$$\boxed{\Gamma = S_{11} + \mathbf{S}^{\mathrm{CA,DUT}} \left(\mathbf{I} - \mathbf{S}^{\mathrm{L}}\mathbf{S}^{\mathrm{DUT,DUT}}\right)^{-1} \mathbf{S}^{\mathrm{L}}\mathbf{S}^{\mathrm{DUT,CA}}} \tag{8}$$

2 Example: Two On-chip Antennas

Next, we consider the specifc case of a two-element DUT array and a diagonal load matrix.

2.1 Measurement Equation

Now, the load matrix simply becomes

$$\mathbf{S}^{\mathrm{L}} = \begin{pmatrix} \Gamma_1^{\mathrm{L}} & 0 \\ 0 & \Gamma_2^{\mathrm{L}} \end{pmatrix} \tag{9}$$

and the DUT array self-scattering matrix

$$\mathbf{S}^{\mathrm{DUT,DUT}} = \begin{pmatrix} S_{22} & S_{23} \\ S_{32} & S_{33} \end{pmatrix} \tag{10}$$

Considering Eq. (8), we thus have that the product

$$\mathbf{S}^{\mathrm{L}}\mathbf{S}^{\mathrm{DUT,DUT}} = \begin{pmatrix} \Gamma_1^{\mathrm{L}} S_{22} & \Gamma_1^{\mathrm{L}} S_{23} \\ \Gamma_2^{\mathrm{L}} S_{32} & \Gamma_2^{\mathrm{L}} S_{33} \end{pmatrix} \tag{11}$$

and therefore

$$\left(\mathbf{I} - \mathbf{S}^{\mathrm{L}}\mathbf{S}^{\mathrm{DUT,DUT}}\right) = \begin{pmatrix} 1 - \Gamma_1^{\mathrm{L}} S_{22} & -\Gamma_1^{\mathrm{L}} S_{23} \\ -\Gamma_2^{\mathrm{L}} S_{32} & 1 - \Gamma_2^{\mathrm{L}} S_{33} \end{pmatrix} \tag{12}$$

whose inverse is straightforward, i.e.,

$$\left(\mathbf{I} - \mathbf{S}^{\mathrm{L}}\mathbf{S}^{\mathrm{DUT,DUT}}\right)^{-1} = \frac{\begin{pmatrix} 1 - \Gamma_2^{\mathrm{L}} S_{33} & \Gamma_1^{\mathrm{L}} S_{23} \\ \Gamma_2^{\mathrm{L}} S_{32} & 1 - \Gamma_1^{\mathrm{L}} S_{22} \end{pmatrix}}{\left(1 - \Gamma_1^{\mathrm{L}} S_{22}\right)\left(1 - \Gamma_2^{\mathrm{L}} S_{33}\right) - \Gamma_1^{\mathrm{L}} S_{23} \Gamma_2^{\mathrm{L}} S_{32}} \tag{13}$$

Furthermore,

$$\mathbf{S}^{\mathrm{DUT,CA}} = \begin{pmatrix} S_{21} \\ S_{31} \end{pmatrix} \tag{14}$$

and so

$$\mathbf{S}^{\mathrm{L}}\mathbf{S}^{\mathrm{DUT,CA}} = \begin{pmatrix} \Gamma_1^{\mathrm{L}} & 0 \\ 0 & \Gamma_2^{\mathrm{L}} \end{pmatrix} \begin{pmatrix} S_{21} \\ S_{31} \end{pmatrix} = \begin{pmatrix} \Gamma_1^{\mathrm{L}} S_{21} \\ \Gamma_2^{\mathrm{L}} S_{31} \end{pmatrix} \tag{15}$$

so that

$$\left(\mathbf{I} - \mathbf{S}^{\mathrm{L}}\mathbf{S}^{\mathrm{DUT,DUT}}\right)^{-1} \mathbf{S}^{\mathrm{L}}\mathbf{S}^{\mathrm{DUT,CA}} = \frac{\begin{pmatrix} \left(1 - \Gamma_2^{\mathrm{L}} S_{33}\right) \Gamma_1^{\mathrm{L}} S_{21} + \Gamma_1^{\mathrm{L}} S_{23} \Gamma_2^{\mathrm{L}} S_{31} \\ \Gamma_2^{\mathrm{L}} S_{32} \Gamma_1^{\mathrm{L}} S_{21} + \left(1 - \Gamma_1^{\mathrm{L}} S_{22}\right) \Gamma_2^{\mathrm{L}} S_{31} \end{pmatrix}}{\left(1 - \Gamma_1^{\mathrm{L}} S_{22}\right)\left(1 - \Gamma_2^{\mathrm{L}} S_{33}\right) - \Gamma_1^{\mathrm{L}} S_{23} \Gamma_2^{\mathrm{L}} S_{32}} \tag{16}$$

In view of Eq. (8), we include one more term:

$$\mathbf{S}^{\mathrm{CA,DUT}} \left(\mathbf{I} - \mathbf{S}^{\mathrm{L}}\mathbf{S}^{\mathrm{DUT,DUT}}\right)^{-1} \mathbf{S}^{\mathrm{L}}\mathbf{S}^{\mathrm{DUT,CA}} = \frac{\begin{pmatrix} S_{21} \\ S_{31} \end{pmatrix}^T \begin{pmatrix} \left(1 - \Gamma_2^{\mathrm{L}} S_{33}\right) \Gamma_1^{\mathrm{L}} S_{21} + \Gamma_1^{\mathrm{L}} S_{23} \Gamma_2^{\mathrm{L}} S_{31} \\ \Gamma_2^{\mathrm{L}} S_{32} \Gamma_1^{\mathrm{L}} S_{21} + \left(1 - \Gamma_1^{\mathrm{L}} S_{22}\right) \Gamma_2^{\mathrm{L}} S_{31} \end{pmatrix}}{\left(1 - \Gamma_1^{\mathrm{L}} S_{22}\right)\left(1 - \Gamma_2^{\mathrm{L}} S_{33}\right) - \Gamma_1^{\mathrm{L}} S_{23} \Gamma_2^{\mathrm{L}} S_{32}} \tag{17}$$

and thus Γ is written as

$$\Gamma = S_{11} + \frac{\begin{pmatrix} S_{21} \\ S_{31} \end{pmatrix}^T \begin{pmatrix} \left(1-\Gamma_2^L S_{33}\right)\Gamma_1^L S_{21} + \Gamma_1^L S_{23}\Gamma_2^L S_{31} \\ \Gamma_2^L S_{32}\Gamma_1^L S_{21} + \left(1-\Gamma_1^L S_{22}\right)\Gamma_2^L S_{31} \end{pmatrix}}{\left(1-\Gamma_1^L S_{22}\right)\left(1-\Gamma_2^L S_{33}\right) - \Gamma_1^L S_{23}\Gamma_2^L S_{32}} \tag{18}$$

that is,

$$\Gamma = S_{11} + \frac{\left(1-\Gamma_2^L S_{33}\right)\Gamma_1^L S_{21}^2 + S_{21}\Gamma_1^L S_{23}\Gamma_2^L S_{31} + S_{31}\Gamma_2^L S_{32}\Gamma_1^L S_{21} + \left(1-\Gamma_1^L S_{22}\right)\Gamma_2^L S_{31}^2}{\left(1-\Gamma_1^L S_{22}\right)\left(1-\Gamma_2^L S_{33}\right) - \Gamma_1^L S_{23}\Gamma_2^L S_{32}} \tag{19}$$

which finally simplifies to

$$\boxed{\Gamma = S_{11} + \frac{\left(1-\Gamma_2^L S_{33}\right) S_{21}^2 \Gamma_1^L + \left(1-\Gamma_1^L S_{22}\right) S_{31}^2 \Gamma_2^L + 2S_{21}S_{31}S_{23}\Gamma_1^L\Gamma_2^L}{\left(1-\Gamma_1^L S_{22}\right)\left(1-\Gamma_2^L S_{33}\right) - S_{23}^2\Gamma_1^L\Gamma_2^L}} \tag{20}$$

2.2 Solving for S-parameters

The objective is to solve for the S-parameters of the 3-port by measuring the reflection coefficient Γ for different DUT loads Γ_1^L and Γ_2^L. To do so, we consider different cases:

- Case 1: $\Gamma_1^L = 0$ and $\Gamma_2^L \neq 0$

Substituting $\Gamma_1^L = 0$ and $\Gamma_2^L \neq 0$ in Eq. (20), we obtain

$$\Gamma = S_{11} + \frac{\Gamma_2^L S_{31}^2}{1-\Gamma_2^L S_{33}} \tag{21}$$

which is identical to the single-port DUT case. To find S_{11}, S_{31}, and S_{33}, we first write the equation as

$$\begin{aligned} \Gamma(1-\Gamma_2^L S_{33}) &= S_{11}(1-\Gamma_2^L S_{33}) + \Gamma_2^L S_{31}^2 \\ \Gamma &= S_{11} + \Gamma\Gamma_2^L S_{33} + \Gamma_2^L\left(S_{31}^2 - S_{11}S_{33}\right) \\ \Gamma &= \begin{bmatrix} 1 & \Gamma\Gamma_2^L & \Gamma_2^L \end{bmatrix} \begin{bmatrix} S_{11} \\ S_{33} \\ S_{31}^2 - S_{11}S_{33} \end{bmatrix} \end{aligned} \tag{22}$$

Next, we consider at least three different loads $\Gamma_2^{L,(n)}$ for $n = 1, 2, 3, \ldots$ and measure the corresponding chamber antenna reflection coefficients $\Gamma^{(n)}$ and solve for

$$\begin{bmatrix} S_{11} \\ S_{33} \\ S_{31}^2 - S_{11}S_{33} \end{bmatrix} = \begin{bmatrix} 1 & \Gamma^{(1)}\Gamma_2^{L,(1)} & \Gamma_2^{L,(1)} \\ 1 & \Gamma^{(2)}\Gamma_2^{L,(2)} & \Gamma_2^{L,(2)} \\ 1 & \Gamma^{(3)}\Gamma_2^{L,(3)} & \Gamma_2^{L,(3)} \\ \vdots & \vdots & \vdots \end{bmatrix}^{\dagger} \begin{bmatrix} \Gamma^{(1)} \\ \Gamma^{(2)} \\ \Gamma^{(3)} \\ \vdots \end{bmatrix} \tag{23}$$

where the dagger denotes the pseudo-inverse. Note that S_{11} and S_{33} are found directly after which S_{31}^2 is solved. And because we are only interested in $|S_{31}|$, the sign-ambiguity will not matter.

- Case 2: $\Gamma_1^L \neq 0$ and $\Gamma_2^L = 0$

Substituting $\Gamma_1^L \neq 0$ and $\Gamma_2^L = 0$ in Eq. (20), we obtain

$$\Gamma = S_{11} + \frac{\Gamma_1^L S_{21}^2}{1-\Gamma_1^L S_{22}} \tag{24}$$

Similar to Case 1, we find S_{11}, S_{21}, and S_{22} by solving for

$$\begin{bmatrix} S_{11} \\ S_{22} \\ S_{21}^2 - S_{11}S_{22} \end{bmatrix} = \begin{bmatrix} 1 & \Gamma^{(1)}\Gamma_1^{\mathrm{L},(1)} & \Gamma_1^{\mathrm{L},(1)} \\ 1 & \Gamma^{(2)}\Gamma_1^{\mathrm{L},(2)} & \Gamma_1^{\mathrm{L},(2)} \\ 1 & \Gamma^{(3)}\Gamma_1^{\mathrm{L},(3)} & \Gamma_1^{\mathrm{L},(3)} \\ \vdots & \vdots & \vdots \end{bmatrix}^{\dagger} \begin{bmatrix} \Gamma^{(1)} \\ \Gamma^{(2)} \\ \Gamma^{(3)} \\ \vdots \end{bmatrix} \tag{25}$$

At this point we found S_{11}, $\pm S_{31}$ (because we found S_{31}^2), S_{33}, $\pm S_{21}$ (because we found S_{21}^2), and S_{22}. To find S_{23} we consider one more case, i.e.,

- Case 3: $\Gamma_1^{\mathrm{L}} \neq 0$ and $\Gamma_2^{\mathrm{L}} \neq 0$

In this case we return to

$$\Gamma = S_{11} + \frac{\left(1 - \Gamma_2^{\mathrm{L}} S_{33}\right) S_{21}^2 \Gamma_1^{\mathrm{L}} + \left(1 - \Gamma_1^{\mathrm{L}} S_{22}\right) S_{31}^2 \Gamma_2^{\mathrm{L}} + 2 S_{21} S_{31} S_{23} \Gamma_1^{\mathrm{L}} \Gamma_2^{\mathrm{L}}}{\left(1 - \Gamma_1^{\mathrm{L}} S_{22}\right)\left(1 - \Gamma_2^{\mathrm{L}} S_{33}\right) - S_{23}^2 \Gamma_1^{\mathrm{L}} \Gamma_2^{\mathrm{L}}} \tag{26}$$

and write it as

$$a S_{23}^2 + b S_{23} + c = 0 \tag{27}$$

where

$$a = \left(S_{11} - \Gamma\right) \Gamma_1^{\mathrm{L}} \Gamma_2^{\mathrm{L}} \tag{28}$$

$$b = -2 S_{21} S_{31} \Gamma_1^{\mathrm{L}} \Gamma_2^{\mathrm{L}} \tag{29}$$

$$\begin{aligned} c = {} & \Gamma \left(1 - \Gamma_1^{\mathrm{L}} S_{22}\right)\left(1 - \Gamma_2^{\mathrm{L}} S_{33}\right) - S_{11}\left(1 - \Gamma_1^{\mathrm{L}} S_{22}\right)\left(1 - \Gamma_2^{\mathrm{L}} S_{33}\right) \\ & - \left(1 - \Gamma_2^{\mathrm{L}} S_{33}\right) S_{21}^2 \Gamma_1^{\mathrm{L}} - \left(1 - \Gamma_1^{\mathrm{L}} S_{22}\right) S_{31}^2 \Gamma_2^{\mathrm{L}} \end{aligned} \tag{30}$$

which has the two solutions

$$S_{23} = \frac{-b \pm \sqrt{b^2 - 4ac}}{2a} \tag{31}$$

We now found S_{11}, S_{33} and S_{31}^2 (Case 1), S_{11}, S_{22} and S_{21}^2 (Case 2), and S_{23} (Case 3). Note the sign-ambiguities for S_{21} and S_{31}, as well as the double solution for S_{23}. These ambiguities are yet to be solved. Furthermore, it is pointed out that we typically use 4 different load terminations, where one load that is close to the middle of the Smithchart will be used for re-normalizing all S-parameters. Accordingly, we can realize $\Gamma^{\mathrm{L}} = 0$, which is needed in the above cases.